The Astronomical Journal, 132:2099–2113, 2006 November
© 2006. The American Astronomical Society. All rights reserved. Printed in U.S.A.

THE ADVANTAGE OF INCREASED RESOLUTION IN THE STUDY OF QUASAR ABSORPTION SYSTEMS

Anand Narayanan,[1] Toru Misawa,[1] Jane C. Charlton,[1] and Rajib Ganguly[2]

Received 2006 May 11; accepted 2006 August 2

ABSTRACT

We compare a new $R = 120,000$ spectrum of PG 1634+706 ($z_{QSO} = 1.337$ and $m_V = 14.9$) obtained with the HDS instrument on Subaru to a $R = 45,000$ spectrum obtained previously with the Keck HIRES. In the strong Mg II system at $z = 0.9902$ and the multiple-cloud, weak Mg II system at $z = 1.0414$, we find that at the higher resolution, additional components are resolved in a blended profile. We find that two single-cloud, weak Mg II absorbers were already resolved at $R = 45,000$, with $b = 2$–4 km s^{-1}. The narrowest line that we measure in the $R = 120,000$ spectrum is a component of the Galactic Na I absorption, with $b = 0.90 \pm 0.20$ km s^{-1}. We discuss expectations of similarly narrow lines in various applications, including studies of damped Lyα absorbers, the Mg I phases of strong Mg II absorbers, and high-velocity clouds. By applying Voigt profile fitting to synthetic lines, we compare the consistency with which line profile parameters can be accurately recovered at $R = 45{,}000$ and 120,000. We estimate the improvement gained from superhigh resolution in resolving narrowly separated velocity components in absorption profiles. We also explore the influence of isotope line shifts and hyperfine splitting in measurements of line profile parameters, and the spectral resolution needed to identify these effects. Superhigh-resolution spectra of quasars, which will be routinely possible with 20 m class telescopes, will lead to greater sensitivity for absorption-line surveys, and to the determination of more accurate physical conditions for cold phases of gas in various environments.

Key words: galaxies: halos — galaxies: ISM — methods: statistical — quasars: absorption lines — quasars: individual (PG 1634+706) — techniques: spectroscopic

Online material: color figure

1. INTRODUCTION

With the advent of high-resolution spectroscopy on 8 m class telescopes in the early 1990s came a revelation in the study of quasar absorption-line systems. Previous to this time, several large surveys were conducted with a typical resolution of $R = \lambda/\Delta\lambda = 1000$–$3000$, corresponding to 100–300 km s^{-1}. These surveys tabulated the redshift path densities of Mg II, C IV, and Lyα lines over the redshift range accessible from optical telescopes (Lanzetta et al. 1987; Sargent et al. 1988; Caulet 1989). However, most individual systems were not resolved, so that the kinematics of the different metal lines could not be compared system by system. It is not surprising that an increase of resolution to $R = 45,000$ ($\sim$7 km s^{-1}) provided detailed views of the multiphase structure of gas inside and around galaxies, since parcels of gas within the different components of galaxies are often moving at several to tens of km s^{-1} relative to one another. The increase of resolution from thousands to tens of thousands also brought a dramatic increase in the sensitivity of surveys. This allowed for measurements of the metallicity in the most diffuse gas sampled by weak Lyα forest lines (e.g., Cowie et al. 1995), and for deeper surveys of metal lines as well (e.g., Churchill et al. 1999; Misawa et al. 2002).

At present, hundreds of quasar spectra have been obtained with $R \sim 45,000$ using the High Resolution Echelle Spectrograph (HIRES) on Keck I (Vogt et al. 1994), the High Dispersion Spectrograph (HDS) on Subaru (Noguchi et al. 2002), and the Ultraviolet-Visual Echelle Spectrograph (UVES) on the Very Large Telescope (VLT; Dekker et al. 2000). There is undoubtedly much to be gained from detailed studies of the absorption lines detected in these databases. However, in this paper we look toward the future and ask what advances we should expect in studies of quasar absorption lines with an increase in resolution from the presently attainable value of 7 km s^{-1} to 0.5–2 km s^{-1}, which is within the reach of 20 m class telescopes for hundreds of quasars. This follows a study by Tappe & Black (2004) of the quasar PKS 2145+067 at $R \sim 100,000$ with UVES on the VLT UT2 telescope. That study focused on the $z = 0.79089$ strong Mg II absorber and measured b-parameters in the range 1–7 km s^{-1}, showing considerably more structure than previous spectra (Churchill & Vogt 2001) with $R \sim 45{,}000$. More recently, Chand et al. (2006) considered the effect of observing at $R > 100{,}000$ for studies of variation in the fine-structure constant.

In addition to the increased sensitivity to weak lines gained at higher resolution, there is reason to expect we should see substructure on km s^{-1} scales. Distinct small-scale structures are seen in the interstellar medium (ISM) of the Milky Way on these velocity scales (Points et al. 2004). Very narrow components, indicating cold clouds, are seen through 21 cm absorption in some damped Lyα (DLA) systems (Lane et al. 2000). Also, detailed models of transitions detected in DLA systems indicate the presence of a cold phase (Wolfe et al. 2003). The large Mg-to-Mg$^+$ ratios in many components of strong Mg II absorbers, most of which are produced by lines of sight through L^* galaxies, could be explained by a cold phase that produces the bulk of the Mg I absorption (Churchill et al. 2003). In the case of the $z = 0.9902$ system toward PG 1634+706, Ding et al. (2003) proposed cold clouds with Doppler parameters of b(Mg) ~ 0.75 km s^{-1} to explain the strong Mg I absorption, but these could not be resolved at FWHM ~ 7 km s^{-1}. Finally, Very Large Array observations of Milky Way high-velocity clouds (HVCs) indicate that they have $T < 900$ K, and most Milky Way lines of sight show narrow Ca II lines from HVCs (Richter et al. 2005). However, at FWHM ~ 7 km s^{-1} these Ca II lines were unresolved. Richter et al. (2005) suggested that if the Milky Way is typical of spiral

[1] Department of Astronomy and Astrophysics, The Pennsylvania State University, University Park, PA 16802; anand@astro.psu.edu, misawa@astro.psu.edu, charlton@astro.psu.edu.

[2] Department of Physics and Astronomy, 1000 East University Avenue, University of Wyoming, Laramie, WY 82071; ganguly@uwyo.edu.

galaxy halos, these narrow absorption features should be commonly seen in the profiles of strong Mg II absorbers and Lyman limit systems.

For the brightest quasars it is already feasible to use the highest resolution settings on 8 m class telescopes ($\sim$40 with $m_V < 16$ for nonexorbitant exposure times) to study quasar absorption-line systems. In this paper we present an exploration of the power of $R = 120,000$ in studying four Mg II absorbers along the line of sight toward the magnitude $m_V = 14.9$ quasar PG 1634+706. Our observations were carried out in the service mode with the HDS on the Subaru Telescope.

The paper begins, in § 2, with a general consideration of how accurately line parameters can be determined at superhigh resolution. In § 3 we present our Subaru HDS observations of several absorption-line systems in the spectrum of one of the brightest quasars, PG 1634+706, and discuss the implications of our $R = 120,000$ observations of these systems. We also show the Milky Way absorption along this line of sight. In § 4 we speculate about the progress that will be made in the study of quasar absorption lines when many quasars are observed at $R > 100{,}000$.

2. SIMULATION OF VERY NARROW ABSORPTION LINES

In gas with temperatures $T < 8000$ K, most metals would produce absorption features that are narrower than $b_{\rm therm} = 2$ km s^{-1}. Figure 1 illustrates progressively narrower absorption profiles of the Mg II λ2796 line with column density $N(\mathrm{Mg}^+) = 10^{12}$ cm^{-2} and Doppler parameters $b(\mathrm{Mg}^+)$ from 9 to 0.01 km s^{-1} at high ($R = 45{,}000$) and superhigh ($R = 120{,}000$) spectral resolutions. The various profiles were produced by convolving a model absorption feature with Gaussian kernels of FWHM = 6.6 and 2.5 km s^{-1} to simulate the resolving powers corresponding to the two spectral resolutions. Comparing the profile shapes, it is apparent that, even at high resolution, the width of intrinsically very narrow lines is often misrepresented. A measurement of b would result in a value significantly higher than the true value, which would further affect the estimation of the upper limit for the gas temperature. To explore the effect of resolution further, we evaluate the consistency with which Voigt profile parameters (i.e., column density and Doppler parameter) can be recovered from very narrow absorption profiles at two resolutions: $R = 120{,}000$ and 45,000 in synthetically simulated spectra. Both these parameters are important for deriving ionization structure, gas-phase metallicities, and other physical conditions for the absorber. In addition, using this approach we also consider two other effects: (1) blending of lines and (2) isotope shifts and hyperfine splitting in absorption lines. We evaluate the advantage of increased resolution in recognizing these effects and also in determining how they influence Doppler parameter measurements of absorption profiles.

2.1. *Very Narrow Single-Component Lines*

For our simulations we synthesized Mg II λ2796 lines with two sets of values: (1) a column density of $N(\mathrm{Mg}^+) = 10^{12}$ cm^{-2} and $b(\mathrm{Mg}^+) = 2.0$ km s^{-1}, corresponding to a rest-frame equivalent-width limit of $W_r(2796\ \text{Å}) = 0.03$ Å, and (2) $N(\mathrm{Mg}^+) = 10^{12}$ cm^{-2} and $b(\mathrm{Mg}^+) = 1.0$ km s^{-1}, corresponding to $W_r(2796\ \text{Å}) = 0.02$ Å. The former characterizes the typically measured profile parameter for the unique class of weak metal-line absorbers known as "single-cloud weak Mg II" systems (Churchill et al. 1999; Rigby et al. 2002; Charlton et al. 2003). The latter would be representative of even colder phases of gas ($T < 1460$ K) at low ionization. Our choice of these values for $b(\mathrm{Mg}^+)$ for the simulations was also motivated by a desire to find the minimum Doppler width at which we expect to resolve lines at $R = 45{,}000$, and to show the improvement with $R = 120{,}000$. Thus, the simulations are driven by the characteristics of the particular instruments that we compare.

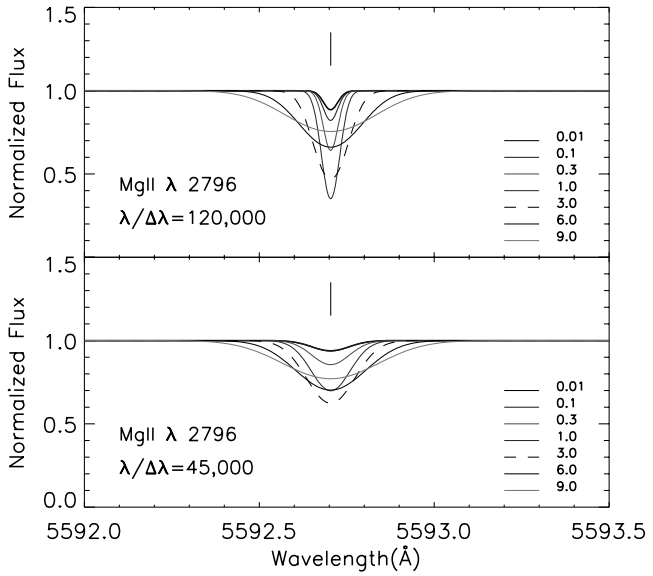

FIG. 1.—Synthetic absorption profiles of varying Doppler parameter b convolved to spectral resolutions of $R = 120{,}000$ and 45,000. The absorption line is redshifted to $z = 1$. The vertical lines mark the center of the absorption profile. [*See the electronic edition of the Journal for a color version of this figure*.]

In generating a synthetic spectrum, an ideal absorption line for the chosen parameters was first simulated using a Voigt function to represent the dependence of absorption on wavelength. The synthetic profile was initially oversampled to assure accurate representation of narrow lines. It was then convolved with a Gaussian instrument kernel, as described above. The convolved profile was then resampled at a rate of 3 pixels per resolution element to enable comparison with observed spectra for a particular R. Finally, Poisson noise was added to the spectra, corresponding to a specified signal-to-noise ratio (S/N) per pixel. To determine the parameters N and b we performed Voigt profile fits on the absorption lines in 10,000 simulated spectra. Figure 2 shows a sample from those simulated lines. The fit parameters were derived by first generating an initial model profile using an automated fitting routine (AUTOVP; Davé et al. 1996) and then adjusting parameters to minimize the χ^2 of that initial model (*minfit*; Churchill 1997), after convolving with the instrumental spread function.

Since we want to evaluate the balance between S/N and resolution, we consider pairs of equal-length exposures with $R = 120{,}000$ and 45,000. The S/Ns were calculated using the relation

$$(\mathrm{S/N})_{45} = (\mathrm{S/N})_{120}\sqrt{\frac{F_{45}\,\delta\lambda_{45} f_{45}(s)}{F_{120}\,\delta\lambda_{120} f_{120}(s)}}, \qquad (1)$$

where F is the expected number of photons incident on the spectrograph slit, $\delta\lambda$ is the grating dispersion (Å pixel^{-1}), and $f(s)$ is the slit throughput for the assumed seeing (s). For simplicity we assume that the incident numbers of photons are the same (i.e., $F_{45} = F_{120}$), although for real systems this is a function of the telescope throughput and collecting area. (We note also that this scaling assumes object-limited observations with negligible contributions from the background and detector read-noise.) We assume that the grating dispersions are 0.04 and

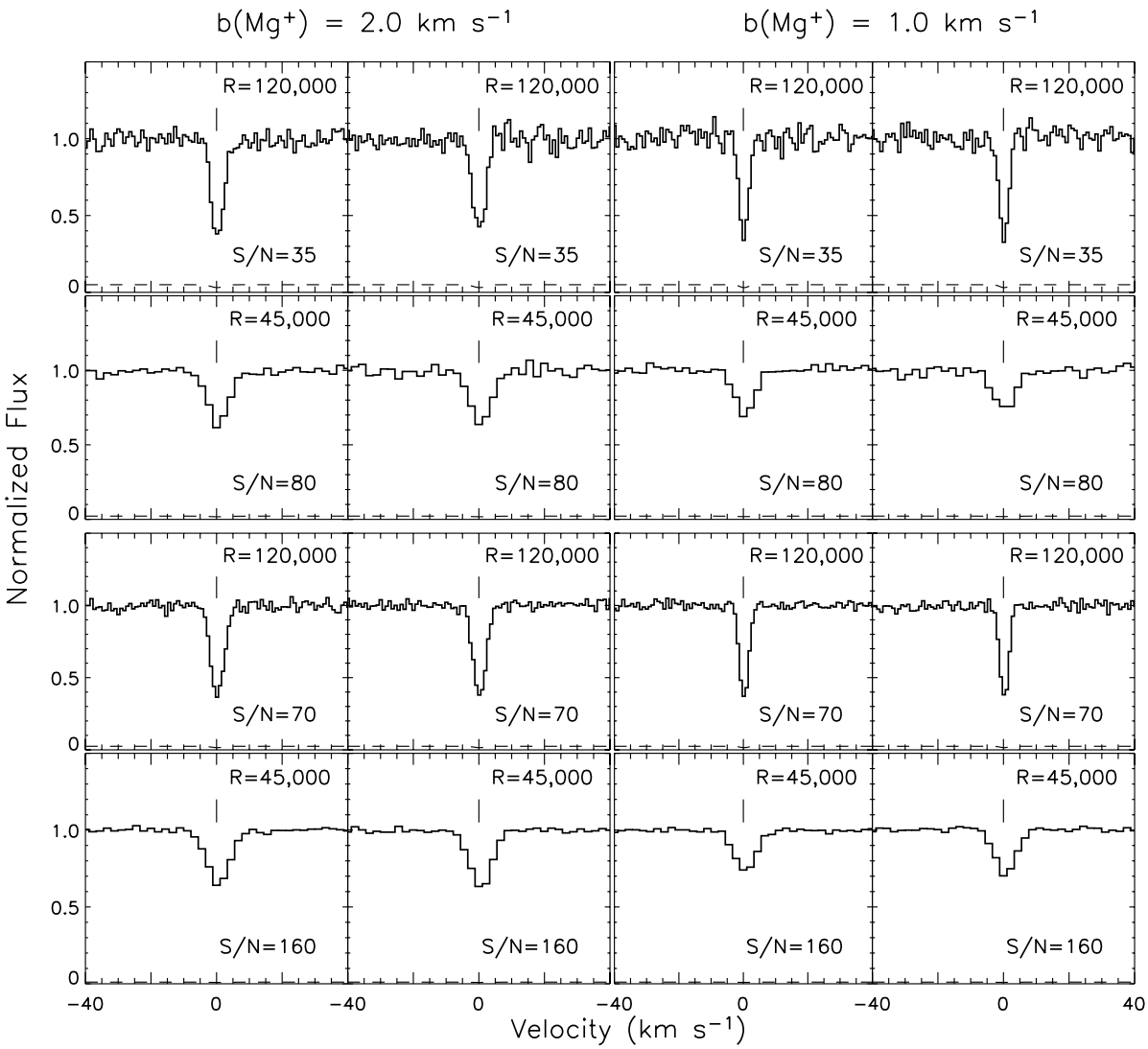

FIG. 2.—Sample from our synthetically simulated Mg II λ2796 absorption lines with noise added. The two sets of lines with Doppler parameters $b(\mathrm{Mg}^+) = 2.0$ km s^{-1} and $b(\mathrm{Mg}^+) = 1.0$ km s^{-1} have a column density of $N(\mathrm{Mg}^+) = 10^{12}$ cm^{-2}. The dashed line at the bottom of each panel is the error spectrum. The vertical lines represent the center of each absorption profile.

0.016 Å for the $R = 45{,}000$ and 120,000 spectra, respectively. To calculate the slit throughput, we consider a seeing of 0.″6 (FWHM, with a Gaussian point-spread function) with slit widths of 0.″861 and 0.″3 for the $R = 45{,}000$ and 120,000 cases. These slit widths were chosen because they represent the two instrumental setups used in our observations of PG 1634+706 with Keck I HIRES and Subaru HDS. In our $R = 120{,}000$ observation of PG 1634+706 using Subaru HDS we were able to obtain a S/N ~ 55 pixel^{-1} for a 1 hr exposure under 0.″6 seeing conditions. Using the relation described above, this scales to a S/N of 128 pixel^{-1} for a spectral resolution of $R = 45{,}000$ for identical exposure time and seeing conditions.

Figure 3 presents the distributions of the measured values of b and N for 10,000 realizations of simulated spectra with $N = 10^{12}$ cm^{-2} and $b = 2.0$ km s^{-1} lines for various combinations of R and S/N. The Doppler parameter characterizes the width of the Voigt profile, which in turn influences the gas temperature estimation. Therefore, we compare the consistency in the measured b-values for each of the 10,000 simulated spectra. For the $R = 45{,}000$ simulations, we find the measured b-values are distributed with a large tail to higher values. The mode of this distribution also falls at a value that is higher than the true b-parameter, and it shifts to even higher values as the S/N is decreased. In a small subset of cases the Voigt profile models from our fitting procedure yielded results that have large formal uncertainties, $\sigma(b)$, in the measurement of b. We find that measurements with $\sigma(b) > b$ are poorly constrained, often with the data in 1 or more pixels deviating by more than 3 σ from the model fit. These models are shown in the distribution plots of Figure 3 as a separate category. For the S/N = 80 case, the small peak at $\sim$0.95 km s^{-1} results from a pixelization effect. Typical line profiles with the appropriate sampling are detected in a small discrete number of pixels ($\sim$1–2), which can lead to bias toward particular values of b. For these profiles the noise also sometimes conspires to produce a b-value even narrower than the instrumental spread function. In such a case the true b-value is likely to be small, but the measurement cannot be claimed as accurate. These simulations therefore reveal the inadequacy of $R = 45{,}000$ data in allowing the recovery of a narrow b-value.

In comparison, for the superhigh-resolution synthetic spectra the distribution of the measured b is significantly narrower, and the mode is very close to the true value. In addition, the intrinsic value remains the most frequently recovered b-parameter even as the S/N is reduced. For the S/Ns that are compared, in almost

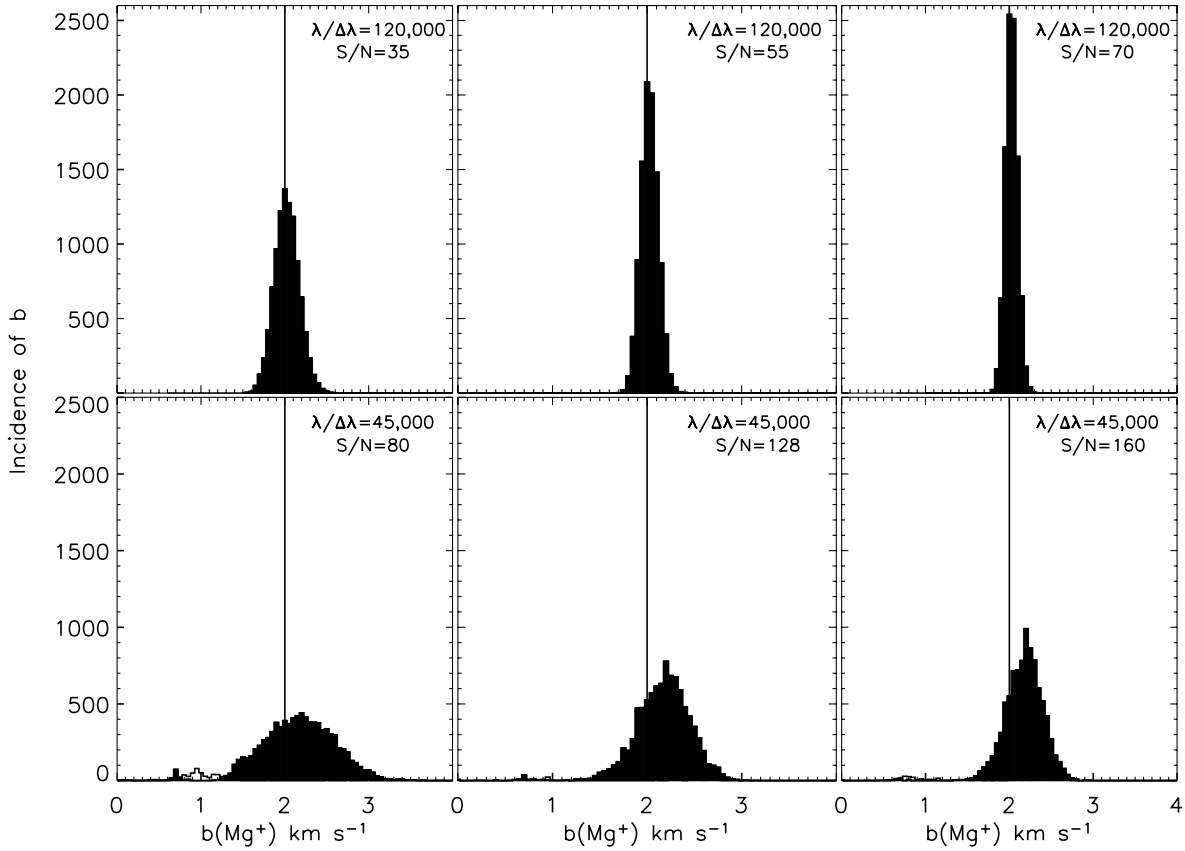

FIG. 3.—Distribution of the measured Doppler parameter b from 10,000 realizations of an Mg II λ2796 line with $W_r(2796\ \text{Å}) = 0.03$ Å. The filled histograms show measurements from well-constrained Voigt profile models that had $\sigma(b) < b$. For each case the measurements that were affected by pixelization are separately shown as open histograms. The true value of the b-parameter is 2.0 km s^{-1}.

all 10,000 cases our fitting procedure gives a well-constrained measurement of the b-value. Table 1 lists, for the various simulations with the two resolutions, the median value of b, with asymmetric 1 σ error bars, and the fraction of Voigt profile fit models with accurate fits [$b > \sigma(b)$]. We conclude that at $R = 120{,}000$ a line profile with a true b-value of 2 km s^{-1} is very accurately recovered. At $R = 45,000$ there is a significantly wider distribution of measurements, with a nonnegligible chance of obtaining b significantly greater than 2 km s^{-1}, and even an occasional measurement of $b \sim 1$ km s^{-1} due to pixelization effects.

Figure 4 shows the distribution of the column density measurements for the same set of simulations. The distributions are broader for the $R = 45{,}000$ case, with mode values smaller than the true value. Measurements thus preserve equivalent width in the sense that a line with an N measurement smaller than the true value will have a measured b larger than the true value. The Voigt profile models that give large $\sigma(b)$ also yield large uncertainties in column density, $\sigma(N)$. Table 1 also summarizes our measurements of N-values for the various simulations. Comparing values in Table 1, it is evident that the constraints from these model fits are poor. We conclude that there is a benefit of observing at $R = 120{,}000$ for lines with $b = 2$ km s^{-1}; however, it is likely that even at $R = 45{,}000$ the derived value will be roughly correct.

The real advantage of higher resolution is for even narrower lines. We performed a similar series of simulations for Mg II λ2796 lines with $N = 10^{12}$ cm^{-2} and $b = 1$ km s^{-1}. The results for the distributions of b-parameters for various S/N values at

TABLE 1
RESULTS FROM SIMULATIONS

		$b(\text{Mg}^+) = 2.0$ km s^{-1}			$b(\text{Mg}^+) = 1.0$ km s^{-1}		
R/1000	S/N (pixel^{-1})	$b(\text{Mg}^+)^*$	$\log N(\text{Mg}^+)^*$	Model Fraction[a] (%)	$b(\text{Mg}^+)^*$	$\log N(\text{Mg}^+)^*$	Model Fraction[a] (%)
120	35	$2.02^{+0.15}_{-0.14}$	$12.0^{+0.02}_{-0.02}$	99.99	$1.07^{+0.16}_{-0.16}$	$11.97^{+0.06}_{-0.04}$	90.21
45	80	$2.15^{+0.43}_{-0.48}$	$11.99^{+0.04}_{-0.03}$	94.33	$1.82^{+0.44}_{-0.33}$	$11.84^{+0.04}_{-0.03}$	44.00
120	55	$2.02^{+0.10}_{-0.09}$	$12.0^{+0.01}_{-0.02}$	99.98	$1.05^{+0.11}_{-0.13}$	$11.97^{+0.05}_{-0.03}$	97.80
45	128	$2.17^{+0.26}_{-0.32}$	$11.98^{+0.03}_{-0.01}$	98.44	$1.56^{+0.35}_{-0.27}$	$11.85^{+0.04}_{-0.02}$	51.86
120	70	$2.02^{+0.08}_{-0.07}$	$12.0^{+0.01}_{-0.01}$	99.98	$1.05^{+0.09}_{-0.10}$	$11.97^{+0.04}_{-0.02}$	98.98
45	160	$2.17^{+0.21}_{-0.25}$	$11.98^{+0.02}_{-0.01}$	98.03	$1.55^{+0.33}_{-0.28}$	$11.86^{+0.03}_{-0.03}$	51.98

NOTE.—Asterisks indicate median b- and N-values.
[a] Out of 10,000 realizations, the percentage of Voigt profile fit models that gave a reliable measurement [$\sigma(b) < b$].

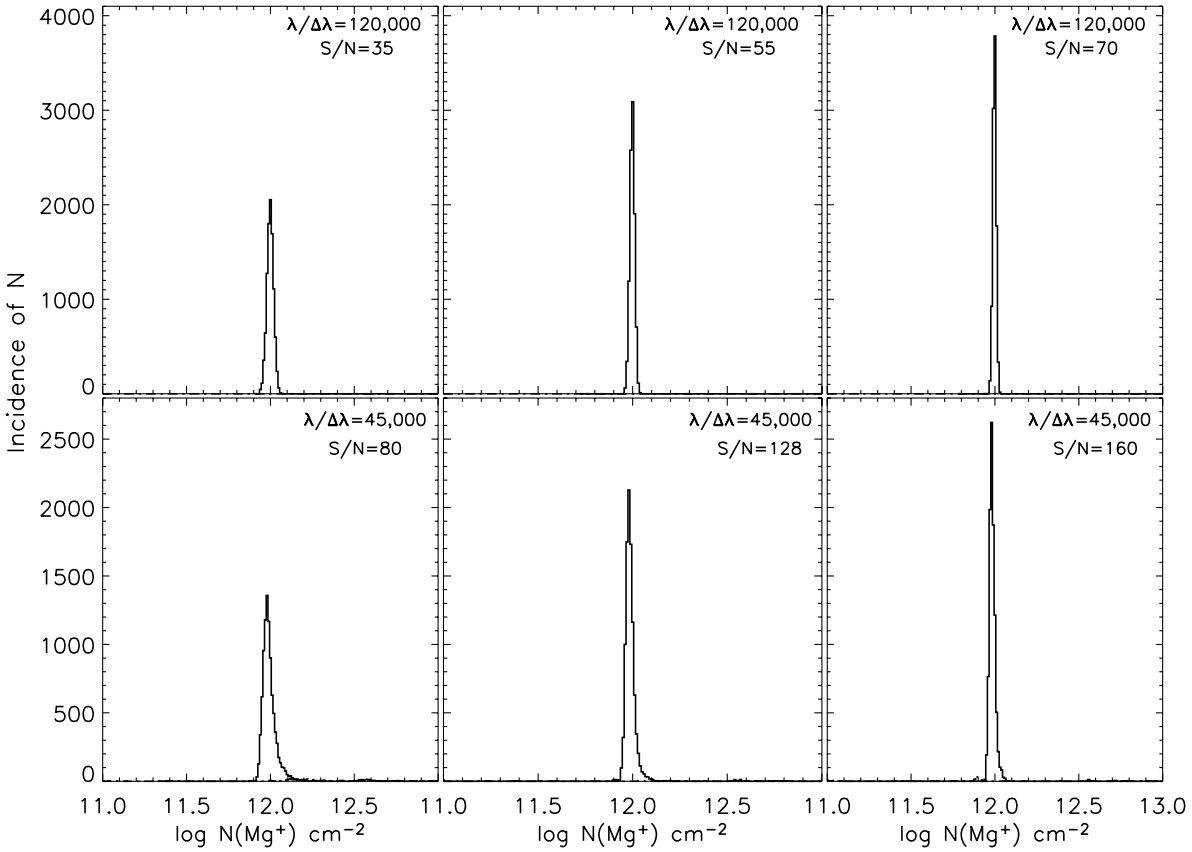

FIG. 4.—Distribution of the measured $N(\mathrm{Mg}^+)$ column density from 10,000 realizations of the Mg II λ2796 line with $W_r(2796\ \text{Å}) = 0.03$ Å. The true value of the column density is $N(\mathrm{Mg}^+) = 10^{12}\ \mathrm{cm}^{-2}$.

$R = 120,000$ and 45,000 are presented in Figure 5. The large spread in the measured value of b for $R = 45,000$ is indicative that this spectral resolution is inadequate to faithfully recover line widths of narrow line profiles. For $R = 45,000$ we again find a large number of measurements with large $\sigma(b)$ values, for a measured b of $\sim$0.95 km s^{-1}. This is again explained by a pixelization effect, but in this case the measurement happens to be very close to the true value. Even if we had chosen a true value of b between 1 and 2 km s^{-1}, this peak would still be at $b \sim 0.95$ km s^{-1}. Nonetheless, a measurement of a small b-value does imply a true narrow line width, even if the measured value is biased by the pixelization.

Even for the $R = 120,000$ spectra, the mode of the distribution for measured b is at a value slightly larger than the true b, although in general the measurements are well constrained. Table 1 lists the median values of Doppler parameters and column densities, and their 1 σ errors, for various S/N values at the two resolutions. The distributions of the N-values are compared in Figure 6.

The significance of increased resolution is clearly seen from Figures 3–6. The determination of b is also sensitive to the sampling, where b greater than roughly a pixel is required. In comparison, the precision in measurements from lower resolutions can be improved only by using substantially higher S/N spectra, thus requiring very long exposure time. Furthermore, we find that similar equivalent-width limits are attained in the $R = 120,000$ and 45,000 spectra for equal exposure lengths even though the S/N of the former is substantially lower. For example, the 5 σ equivalent-width limit for $R = 45,000$, S/N = 80 and $R = 120,000$, S/N = 35 is 5 mÅ pixel^{-1}. Also, as we discuss in §§ 2.2 and 3, observations with $R = 120,000$, corresponding to a resolution of 2.5 km s^{-1}, are very important for resolving lines and separating velocity substructures.

2.2. *Blending of Lines*

To probe the nature of small-scale structure in absorbers it is essential to resolve closely separated velocity components. Here we focus on making estimates of the scale at which superhigh resolution offers a real improvement over intermediate-resolution spectra. We chose a simple scenario of two absorbing clouds, with different physical properties, marginally separated in velocity. The column densities and Doppler parameters of the simulated lines were selected to match closely with those of the weak multiple-cloud system at $z = 1.0414$ in the spectrum of PG 1634+706, so our choice is not completely arbitrary. This multiple-cloud system is discussed in § 3.3. The two components have column densities $N(\mathrm{Mg}^+)$ of 10^{12} and $10^{11.5}$ cm^{-2} and Doppler parameters $b(\mathrm{Mg}^+)$ of 4.0 and 3.0 km s^{-1}, respectively. This corresponds to an equivalent-width ratio of approximately 3 : 1 between the two components. In a set of 1000 simulations with a S/N of 80 pixel^{-1} at $R = 45,000$ and with the two clouds separated in velocity by $\Delta v = 10$ km s^{-1}, we found that in $\sim$84% of the cases Voigt profile fitting was able to distinguish the two components in the absorption profile. For the same S/N and the velocity separation reduced to $\Delta v = 7$ km s^{-1}, in $\sim$95% of the cases the simulated line was fitted with just a single broad Voigt profile with a mean value of $\langle b(\mathrm{Mg}^+)\rangle = 6.3$ km s^{-1}. This translates to a larger upper limit for the estimated temperature of the gas ($T < 58,000$ K) compared to the true value of $T < 20,000$ K. For lines with the same intrinsic properties, but simulated at $R = 120,000$ and S/N = 35 pixel^{-1} (corresponding to an identical exposure time), we found that Voigt profile fits recovered

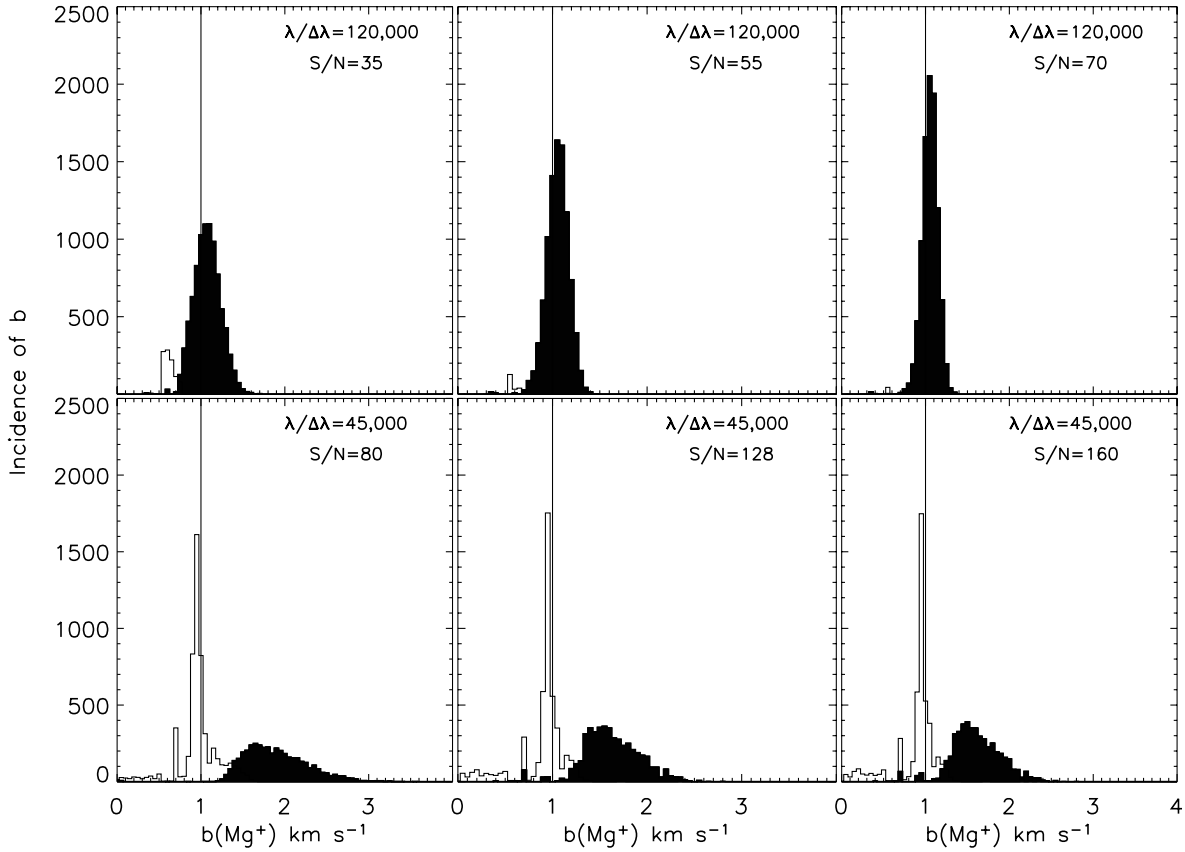

FIG. 5.—Distribution of the measured Doppler parameter b from 10,000 realizations of an Mg II λ2796 line with $W_r(2796\ \text{Å}) = 0.02$ Å. The filled histograms show measurements from well-constrained Voigt profile models that had $\sigma(b) < b$. For each case the measurements that were affected by pixelization are separately shown as open histograms. The true value of the b-parameter is 1.0 km s^{-1}.

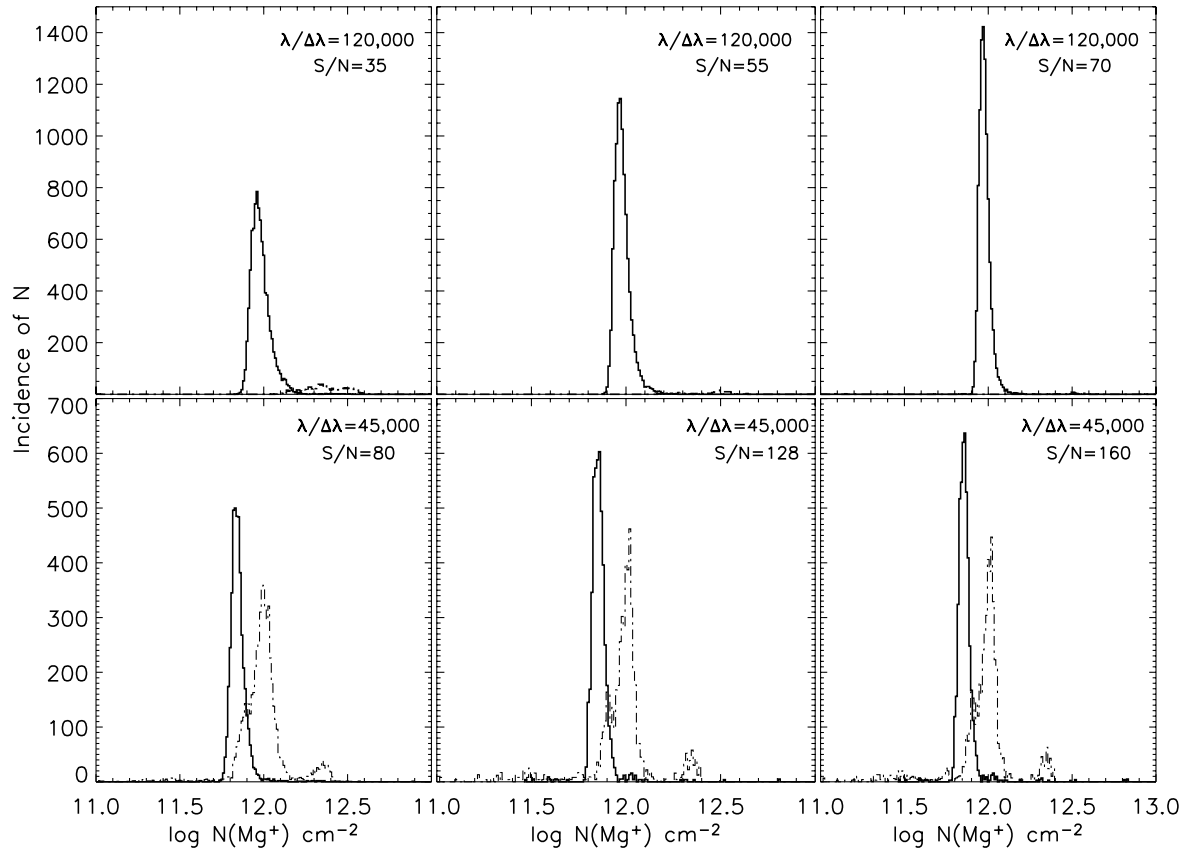

FIG. 6.—Distribution of the measured $N(\text{Mg}^+)$ column density from 10,000 realizations of the Mg II λ2796 line with $W_r(2796\ \text{Å}) = 0.02$ Å. The dash-dotted histograms show measurements that yielded poor constraints [$\sigma(b) > b$]. The true value of the column density is $N(\text{Mg}^+) = 10^{12}$ cm^{-2}.

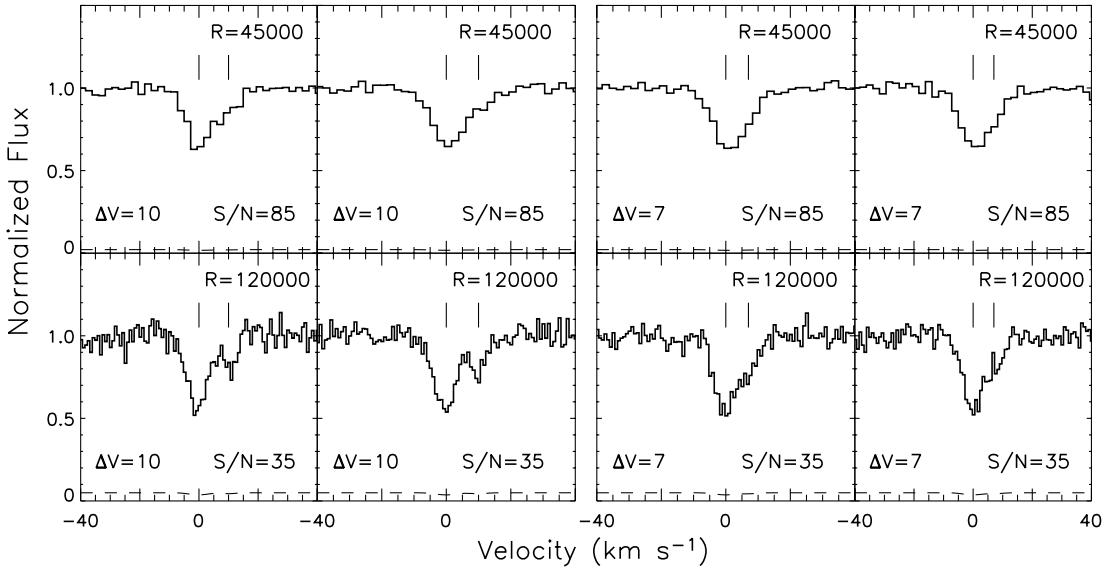

FIG. 7.—Sample showing closely blended synthetically simulated Mg II λ2796 lines with noise added corresponding to a particular S/N. The subpanels in the left panel correspond to the two absorbing components separated in velocity by 10 km s^{-1}. The right panel shows sample simulated spectra illustrating the case in which the two absorbing components are separated in velocity by 7 km s^{-1}. The vertical lines mark the position of the two components. The S/Ns for the two resolutions are estimated for equal exposure times.

both kinematic components in ~97% of the cases with a velocity separation of $\Delta v = 7$ km s^{-1}, and in 100% of the cases with the velocity separation increased to $\Delta v = 10$ km s^{-1}. Furthermore, increasing the S/N of the intermediate-resolution spectra did not compensate for the lower resolution. For example, when the two components were separated in velocity by 7 km s^{-1}, even with S/N = 160 pixel^{-1} at $R = 45{,}000$, the kinematically separate components were resolved only in ~40% of the cases. Figure 7 shows a sample of the simulated lines at the two resolutions. From these results we infer that even at fairly high S/Ns, intermediate resolutions can be completely inadequate in revealing closely blended velocity structures on scales smaller than 8 km s^{-1}. Further, such unresolved lines can lead to overestimation of the temperature of the absorbing gas. More generally, we conclude that if two lines are narrower than their velocity separation, they can be resolved by a Voigt profile fit if the resolution is less than ~70% of the velocity separation. The exact criterion for separating blends is dependent on the quality of the spectra and the Doppler parameters of the two lines.

2.3. *Contribution from Isotopes and Hyperfine Splitting*

Magnesium has three isotopes with mass numbers 24, 25, and 26 amu, with relative abundances of 78.99%, 10.00%, and 11.01%, respectively. The wavelengths of the resonance lines for these isotopes differ from one another. Furthermore, ^{25}Mg shows hyperfine splitting. The relative shifts in rest-frame wavelength for each line of the resonance doublet are measured to be $\lambda_{24} - \lambda_{25}^{+} = 0.0014$ Å, $\lambda_{24} - \lambda_{25}^{-} = 0.0061$ Å, and $\lambda_{24} - \lambda_{26} = 0.008$ Å (Morton 2003). In velocity space this corresponds to 0.1500, 0.6540, and 0.8577 km s^{-1}, respectively. For such narrow velocity separations, the effect of isotope shifts and hyperfine splitting becomes distinguishable only at extremely high spectral resolutions ($R > 500{,}000$), as illustrated in Figure 8. To estimate the scale at which this effect is likely to influence our b-value measurements, we simulated very narrow synthetic lines with true $b(^{24}\mathrm{Mg}^{+})$ of 0.3, 0.7, and 1.5 km s^{-1}. The b-values of the other isotope lines were thermally scaled. The simulated lines had S/N = 35 pixel^{-1} at $R = 120{,}000$. Figure 9 shows the dispersion in the incidence of measured b for the various cases. Of the 10,000 simulated lines with $b(^{24}\mathrm{Mg}^{+}) = 0.3$ km s^{-1}, only ~10% of the measurements yielded a b-value less than 0.5 km s^{-1}, with the recovered b-value almost always larger than the true value. For a higher true b-value of 0.7 km s^{-1}, the measurements were still distributed across a range from 0.7 to 1.5 km s^{-1}. The peak of this distribution, however, was closer to the true value than the previous case. For the final case, with $b = 1.5$ km s^{-1}, the spectral resolution became adequate to repeatedly measure values close to the true b-value along with consistently yielding measurements that were reliable [$\sigma(b) < b$]. In this case, although the isotope and hyperfine lines were still contributing to the final absorption profile, their contribution did not induce a significant change in the line width, as the individual line widths were now larger than the largest separation between the isotope lines.

With these results we infer that isotopic line shifts and hyperfine splitting are to be considered as influencing our measurements only when the true line width is really narrow [$T < 700$ K and $b(\mathrm{Mg}^{+}) < 0.7$ km s^{-1}]. Furthermore, for such narrow Mg II lines, identifying the effect would require spectral resolutions of $R > 500{,}000$.

3. SUPERHIGH-RESOLUTION OBSERVATION OF PG 1634+706

We obtained a superhigh-resolution spectrum of PG 1634+706 with the HDS (Noguchi et al. 2002) on Subaru. Using a 0.″3 slit width we were able to attain an $R = 120{,}000$ spectrum with a sampling rate of 3 pixels per resolution element. Our 1 hr observation yielded a spectrum with an average S/N ~ 30 pixel^{-1} over the entire spectral range. The reduced one-dimensional spectrum was extracted in the standard manner with the IRAF software.[3] Wavelength calibration was done using a standard Th-Ar spectrum. The spectrum was continuum fitted with a third-order cubic spline function and normalized. Previously identified weak

[3] IRAF is distributed by the National Optical Astronomy Observatory, which is operated by the Association of Universities for Research in Astronomy, Inc., under cooperative agreement with the NSF.

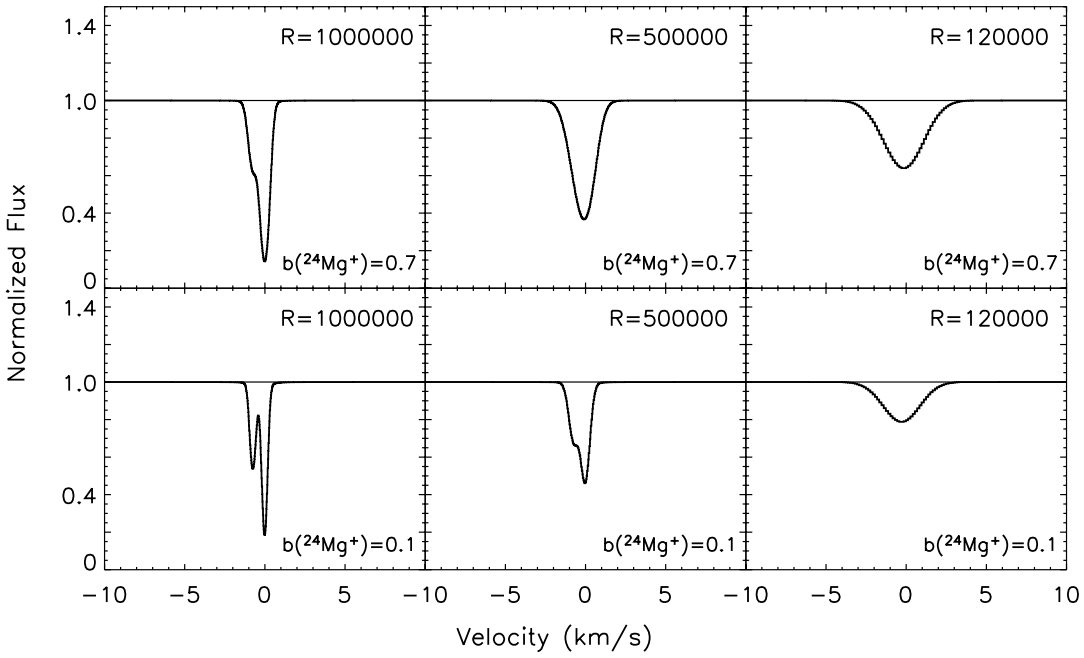

FIG. 8.—Synthetic spectra involving isotope and hyperfine lines, without adding Poisson noise. The Mg II line is redshifted to $z = 1$. A column density of $N(\mathrm{Mg}^+) = 10^{11.5}$ cm^{-2} was assumed. The b-parameter is quoted in units of km s^{-1}. The line asymmetry because of isotopic line shift becomes distinguishable at spectral resolution $R > 500{,}000$ and also when the Doppler width is smaller.

and strong Mg II absorption systems in a $R = 45{,}000$ Keck HIRES spectrum of PG 1634+706 made this observation an ideal test case. The HIRES data acquisition and reduction procedure is described in Churchill & Vogt (2001). The short exposure on HDS reached an equivalent-width limit several times smaller than our exposure of twice its length with the HIRES instrument at a lower resolution of $R = 45{,}000$. Details of the two observations are listed in Table 2. Figure 10 shows the wavelength regions covered in both the HDS and HIRES spectra.

In the following subsections we compare detections of the strong, single-cloud weak, and multiple-cloud weak Mg II absorption features in the superhigh-resolution HDS and the high-resolution HIRES spectra for this quasar. We also consider the Milky Way absorption along this line of sight. We discuss the particular cases of these systems but also generally discuss how studies of the same type of system would be affected by higher resolution observations. Since the scope of this paper is to compare observations taken at different spectral resolutions, we defer detailed analyses of the absorption-line systems presented herein to future work.

3.1. *Strong* Mg II *Absorber at* $z = 0.9902$

The $z = 0.9902$ system along the line of sight to the quasar PG 1634+706 has previously been studied using a combination of the $R = 45,000$ Keck HIRES spectrum and data from the *Hubble Space Telescope* (*HST*) FOS (Churchill et al. 2000; Charlton et al. 2000) and *HST* STIS (Ding et al. 2003). Churchill et al. (2003) found that this strong Mg II doublet could be adequately

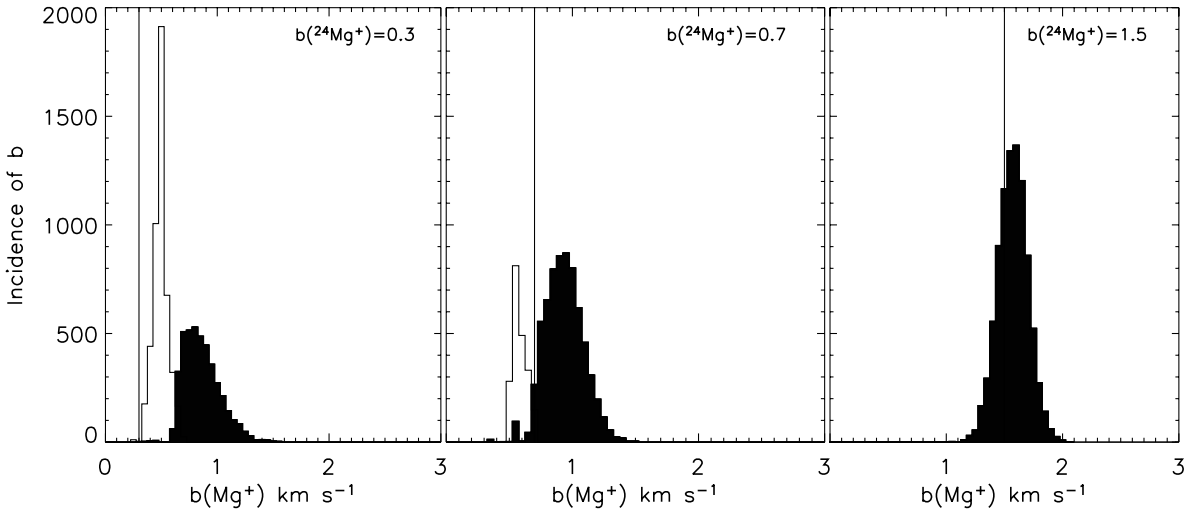

FIG. 9.—Distribution of the measured Doppler parameter from 10,000 realizations of Mg II λ2796 involving the isotopic and hyperfine lines of magnesium. The open histograms show measurements with poor constraints [$\sigma(b) > b$]. The vertical lines show the true b-value assigned to $^{24}\mathrm{Mg}^+$ in each of the three cases. The b-parameter is quoted in units of km s^{-1}.

TABLE 2
PG 1634+706 Observations

Instrument	Resolution ($\lambda/\Delta\lambda$)	Δv (km s^{-1})	Date(s) of Observation	T_{exp} (s)	Coverage (Å)	PI
Keck HIRES	45,000	6.6	1994 Jul 4	2700	3723–6185	C. W. Churchill
	45,000	6.6	1994 Jul 5	5400	3723–6185	C. W. Churchill
Subaru HDS.....	120,000	2.5	2005 Jun 6	3600	4830–7560	T. Misawa

Note.—For $z_{QSO} = 1.337$ and $m_V = 14.9$.

fitted with five blended components. With the higher resolving power of HDS, additional kinematic components were revealed in the Mg II absorption feature. Our Voigt profile fit decomposes the Mg II $\lambda\lambda$2796, 2803 profile into seven components. Figure 11 shows the HIRES and HDS data, comparing differences in the profile shapes for the two resolutions. The asymmetrical shapes for the Mg II λ2796 line at $\Delta v \sim 22$ and $\sim$8 km s^{-1} from the flux-weighted system center in the HIRES spectrum are indicative of narrowly blended features that are clearly distinguished in the profiles in the HDS spectrum. Table 3 presents our Voigt fitting parameters for Mg II $\lambda\lambda$2796, 2803 from the Keck HIRES and Subaru HDS observations. This ability of superhigh resolution to resolve additional components in strong metal-line absorbers was also noted by Chand et al. (2006).

Strong Mg II absorption systems usually have absorption from gas in different phases (different densities and temperatures) residing within an impact parameter of 35 h^{-1} kpc of a luminous galaxy with $L > 0.05L^*$ (Bergeron & Boissé 1991; Steidel et al. 1997). Dissecting the Mg II absorption profile to reveal kinematic structures at small velocity separations of $\Delta v < 1$ km s^{-1} is therefore useful in developing a physical understanding of the spatial distribution of gas in galaxies along the line of sight. If the observed Mg II absorption signatures are characteristic of disk ISM (Lanzetta & Bowen 1992; Charlton & Churchill 1998),

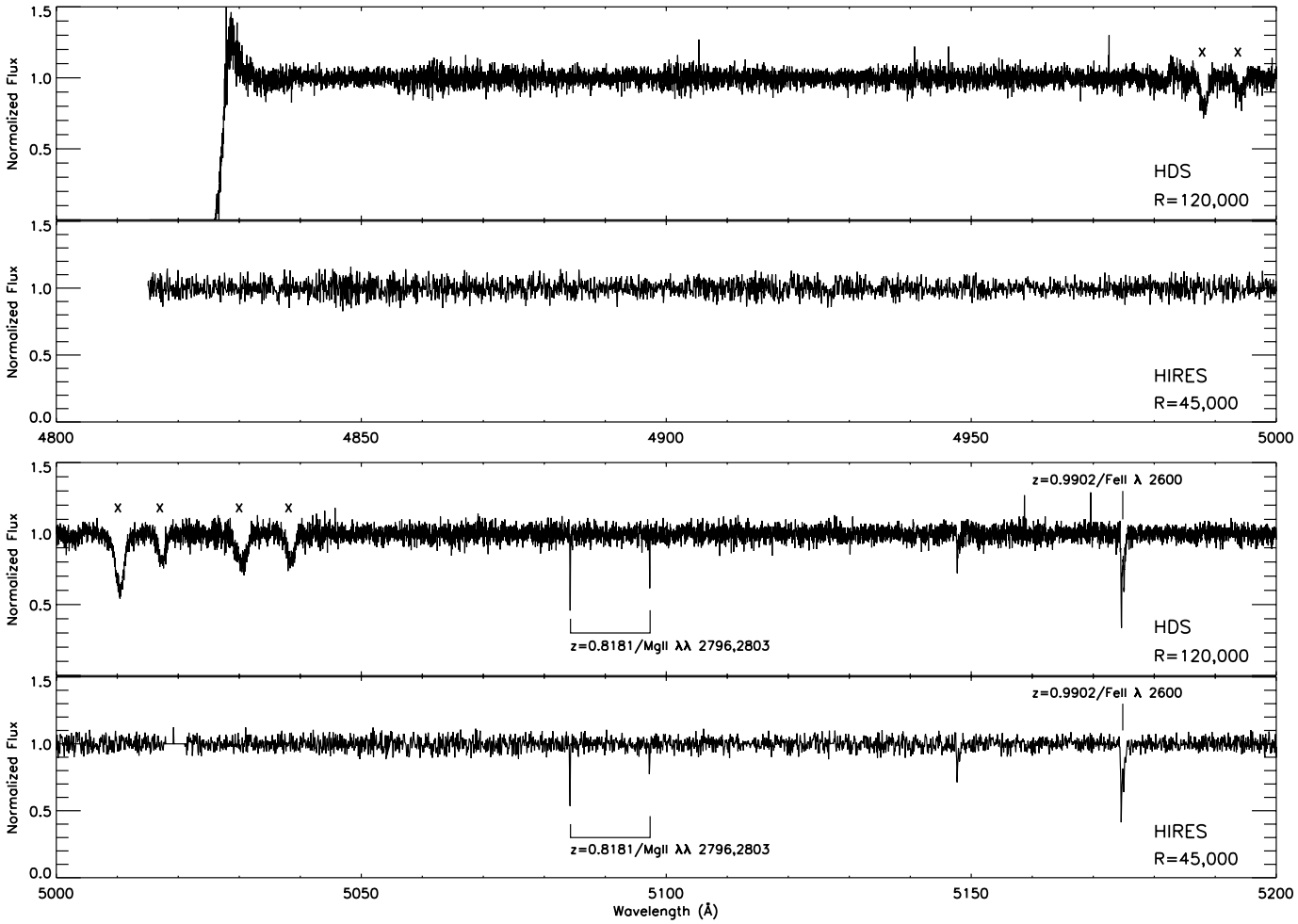

Fig. 10*a*

Fig. 10.—Comparison of PG 1634+706 observations using $R = 120{,}000$ Subaru HDS and $R = 45{,}000$ Keck HIRES. The details of the observations are listed in Table 1. The metal lines associated with the absorption systems discussed in this paper are identified and labeled in both spectra. The features in the HDS spectra marked with crosses are not real and were produced by bad regions in the CCD.

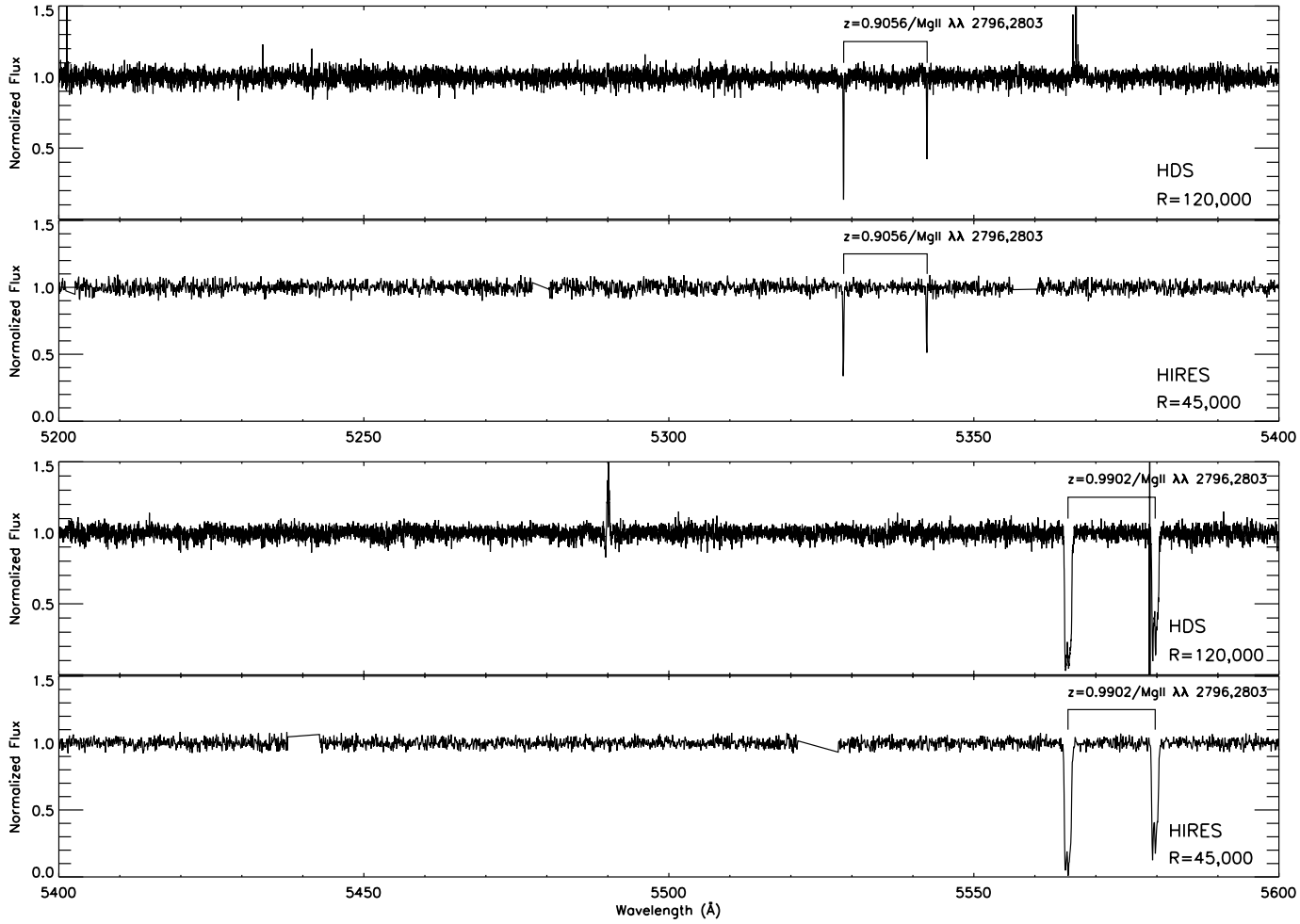

FIG. 10*b*

then measuring structure on the smallest scales is important to determining whether the ISM of high-redshift galaxies follows a complex fractal structure similar to that of the Milky Way (e.g., Elmegreen 1997). Resolving closely blended components, as in the $z \sim 0.9902$ system, is also essential in developing ionization models that provide strong constraints on physical parameters. This is especially relevant when there is a difference or gradient in metallicity, abundance pattern, or ionization from cloud to cloud.

Churchill et al. (2003) studied 23 Mg II systems at $z \sim 1$ and found that many strong Mg II systems have observed column density ratios of $N(\mathrm{Mg})/N(\mathrm{Mg}^{+}) > 0.01$. This value is the maximum expected if the absorption is taking place in gas at a single phase under photoionization equilibrium. In developing a model for this $z = 0.9902$ absorption system based on the $R = 45,000$ Keck HIRES observations, Ding et al. (2003) found that the Mg I absorption line in this system is too strong to arise in the same phase as Mg II for all possible ionization parameters. To reconcile this discrepancy, Ding et al. (2003) invoked an additional lower ionization phase that gave rise to the majority of Mg I absorption but that produced small amounts of Mg II. The lower ionization phase also produced most of the neutral hydrogen absorption from this system, with a range $17.3 < \log N(\mathrm{H}) < 17.7$ for the five Mg I clouds. In this model the Mg I phase gas has a very low temperature ($T \sim 800$ K and $b \sim 0.75$ km s^{-1}), high density ($n_{\mathrm{H}} \sim 200$ cm^{-3}), and small size ($\sim$100 AU), reminiscent of a cold pocket embedded in a warm, ionized intercloud medium as in the ISM of galaxies. The spectral resolution of HIRES was inadequate to show the narrow line widths that we might expect from such cold, small-scale clumps of gas. However, the present Subaru HDS spectrum provides a direct test of the Ding et al. (2003) prediction for this $z = 0.9902$ absorber.

Figure 12 shows the absorption from Mg I λ2853 in the $z = 0.9902$ system, as seen in the HDS spectrum. The Voigt profile fit constraints on the various line features are listed in Table 3. For the three clouds used to fit the Mg I profile, the line widths are not as small as what Ding et al. (2003) had predicted in their models (see their Table 1). For the line width predicted by their model, the Mg I absorption has to be from gas at temperature $T < 800$ K. Our simulation results from § 2.3 show that in instances in which the true b-value is very small, Voigt profile measurements can yield higher values because of unresolved isotopic lines. To investigate whether our measurements of the b-value for the various components of Mg I are influenced by this effect, we resort to simulations. The isotopic lines of Mg I occur at $\lambda_{24} = 2852.9635$ Å, $\lambda_{25} = 2852.9655$ Å, and $\lambda_{26} = 2852.9674$ Å (Beverini et al. 1990). The Mg I λ2853 line does not have hyperfine structure. In our simulations we used the profile parameters predicted by the model [$N(\mathrm{Mg}) = 10^{11.1}$ cm^{-2} and $b(\mathrm{Mg}) = 0.75$ km s^{-1}] for the isotopic line of ^{24}Mg, with the b-parameters of the other two isotopic lines thermally scaled. The spectra were simulated for a S/N = 35 pixel^{-1} at $R = 120,000$, with the lines redshifted to match the redshift of the system. Figure 12 shows the distribution in the incidence of measured b from a simulation of 1000 lines. It can easily be noticed that, although the measured

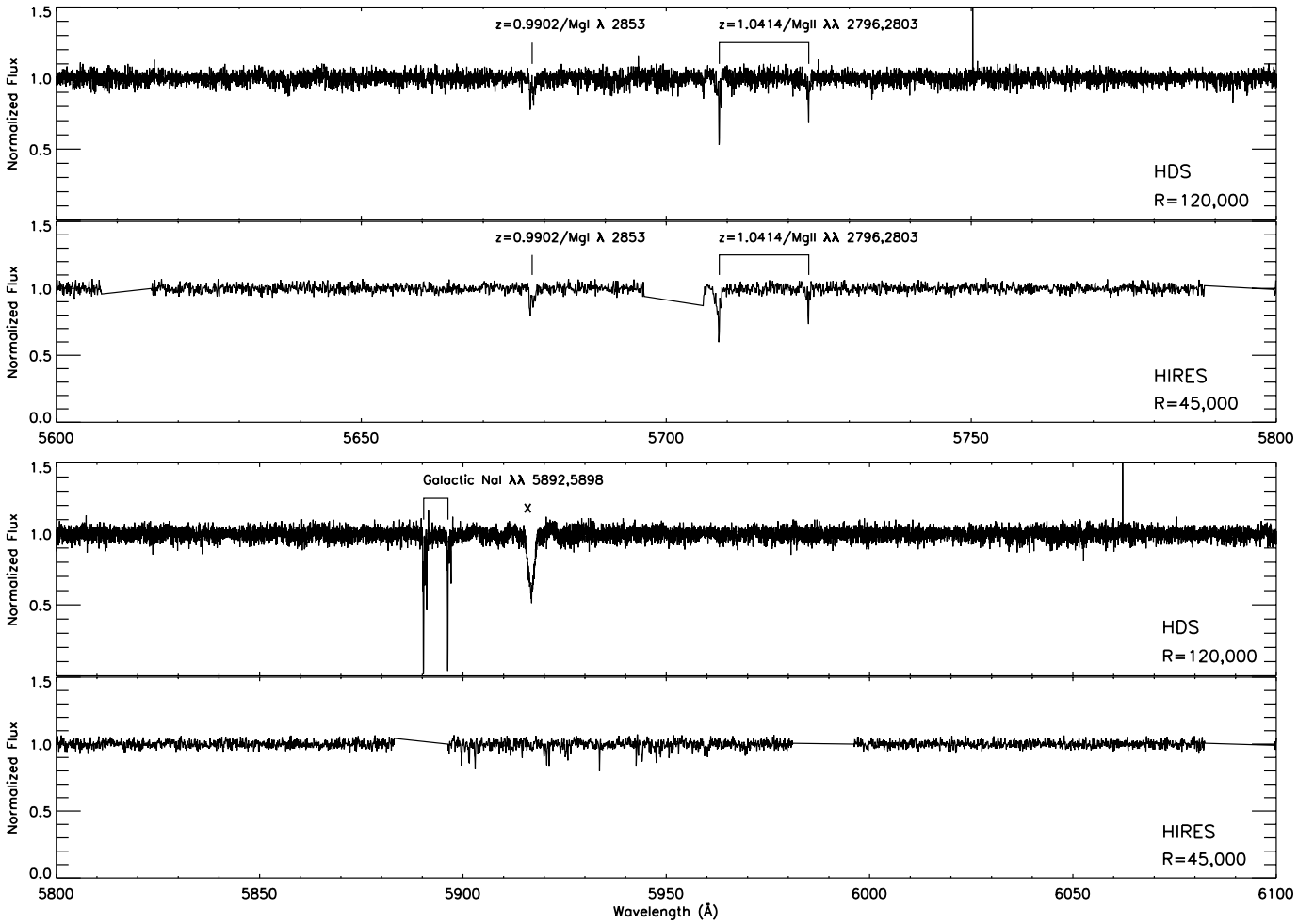

FIG. 10*c*

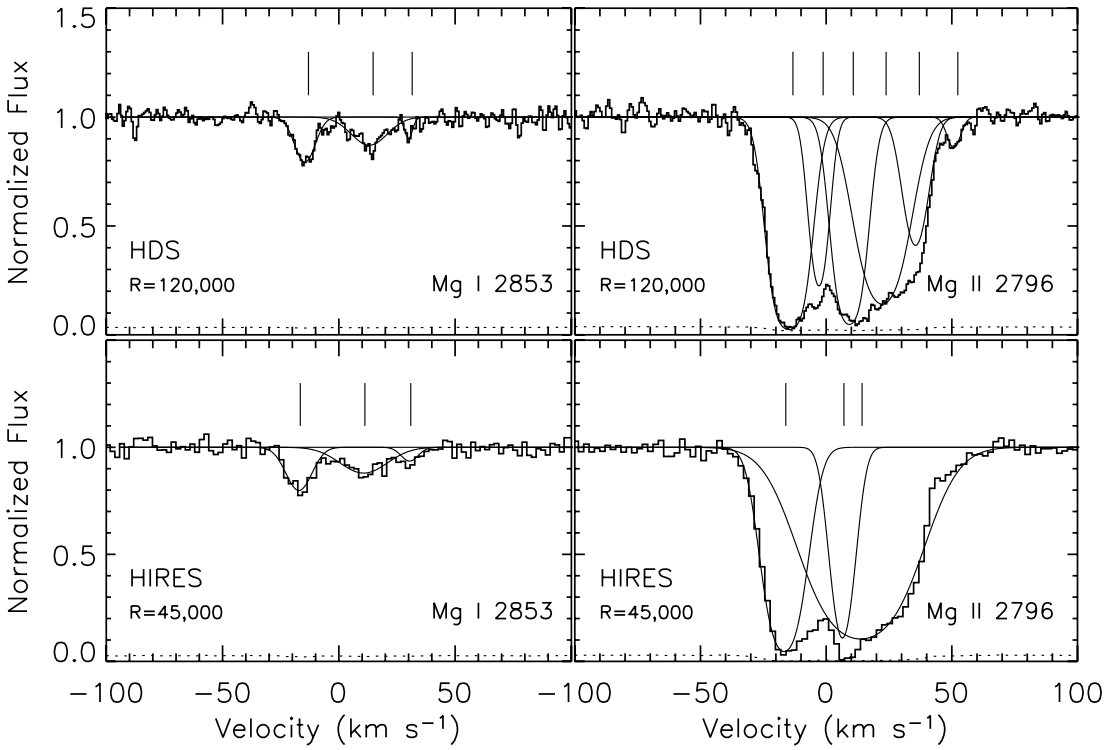

FIG. 11.— The $z = 0.9902$ strong Mg II system as captured by the Keck HIRES and Subaru HDS spectra of PG 1634+706. The left panels show the low-ionization Mg I feature associated with this strong system. The thin solid lines superposed on the spectra are the various Voigt profile components contributing to the absorption feature. The vertical lines placed above the features represent the center of each component. The dotted lines show the error spectra. The results from the Voigt profile fits are listed in Table 3.

TABLE 3
VOIGT PROFILE FIT RESULTS FOR $z = 0.9902$ STRONG Mg II SYSTEM

Instrument	v (km s^{-1})	log N (atoms cm^{-2})	b (km s^{-1})
	Mg I Fit Results		
HIRES	−22.6	11.35 ± 0.04	6.52 ± 0.71
	5.2	11.37 ± 0.06	13.52 ± 2.44
	25.0	10.65 ± 0.18	3.2 ± 2.52
HDS	−20.1	11.26 ± 0.03	5.87 ± 0.46
	7.7	11.28 ± 0.04	10.55 ± 1.28
	24.5	10.51 ± 0.10	5.87 ± 0.94
	Mg II Fit Results		
HIRES	−22.1	13.04 ± 0.01	7.72 ± 0.09
	1.1	12.82 ± 0.01	4.11 ± 0.12
	8.3	13.30 ± 0.01	22.29 ± 0.21
HDS	−20.2	13.05 ± 0.01	7.57 ± 0.15
	−8.2	12.44 ± 0.06	4.46 ± 0.48
	3.8	12.90 ± 0.22	6.50 ± 1.00
	16.8	12.93 ± 0.34	11.03 ± 8.00
	30.1	12.34 ± 0.55	6.11 ± 1.91
	45.4	11.34 ± 0.09	3.37 ± 0.69

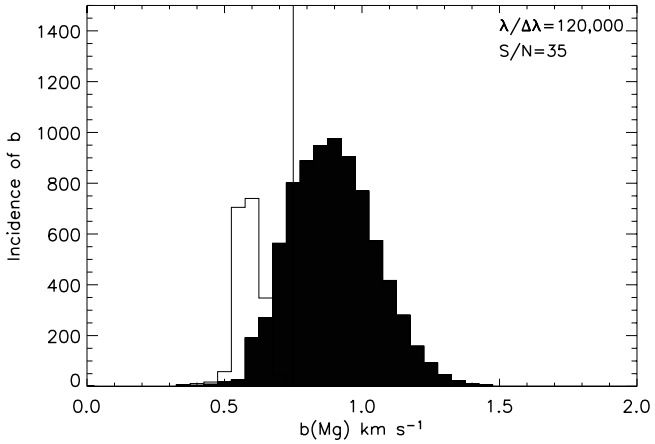

FIG. 12.—Distribution of the measured b-parameter from 10,000 realizations of Mg I λ2853 by considering the isotopic lines of magnesium. The open histogram includes measurements that yielded poor constraints [$\sigma(b) > b$]. The vertical line shows $b(^{24}\mathrm{Mg}) = 0.75$ km s^{-1}, which is the true Doppler parameter for that line. The line was chosen to have a column density of $N(\mathrm{Mg}) = 10^{11.1}$ cm^{-2} to match the model predicted by Ding et al. (2003).

b is almost always larger than the true b of 0.75 km s^{-1}, a measurement of 2 km s^{-1} or higher (as in the observed HDS spectrum) never occurs. It is therefore to be concluded that the hypothesis of a two-phase structure as an explanation of the Mg-to-Mg$^+$ ratio is therefore not consistent with the high-resolution observations. It is clear from § 2 that a component with $b = 0.75$ km s^{-1} will not be measured to have b as high as several km s^{-1} at $R = 120{,}000$. Therefore, another explanation must be sought for this system. Tappe & Black (2004) suggested that a UV flux contribution from the absorbing galaxy and/or Mg + H$^+$ charge transfer could significantly influence the Mg-to-Mg$^+$ ratio. Their $R = 100{,}000$ VLT UVES observation of a different system, at $z = 0.79089$ toward PKS 2145+067, yields $b(\mathrm{Mg}^+) = 1.02 \pm 1.65$ km s^{-1} for the one component detected in Mg I in a spectral region with S/N ∼ 30. The error is too large to draw a conclusion in that case. Another possibility for the $z = 0.9902$ system is that there are more components in the Mg I than we are able to resolve.

We conclude that our $R = 120{,}000$ spectrum does not provide support for a cold-phase model for the $z = 0.9902$ system, although some modified version could apply. Direct tests with superhigh resolution for other similar systems are needed. One excellent candidate is the $z = 0.4523$, multiple-cloud, weak Mg II system toward the quasar HE 0001−2340 ($z = 2.28$ and $m_V = 16.7$), which has detected Fe I and Ca I, as well as Mg I (T. Jones et al. 2006, in preparation). Cold-phase models may also have significant consequences for the study of DLAs and sub-DLAs. Lane et al. (2000) have resolved narrow components ($b \sim 2$–3 km s^{-1}) in an H I 21 cm study of the DLA system at $z = 0.0912$ toward B0738+313. Mg I lines in these systems are expected, from thermal scaling, to be significantly narrower. Also, more recently Srianand et al. (2005) reported measuring a kinetic temperature of ∼150 K from H_2 lines in three DLAs. Such a low gas-phase temperature can produce narrow metal lines, with Doppler widths of ∼3 km s^{-1}, that can be accurately recovered with superhigh-resolution spectra. A fair fraction of DLAs have detected molecules (e.g., Petitjean et al. 2000), indicating directly that they have a cold phase. Other DLAs and Lyman limit systems may also be produced by lines of sight through cold regions surrounding molecular clouds, or regions that did not quite reach the threshold for star formation.

3.2. *Single-Cloud, Weak* Mg II *Absorbers*

Most single-cloud, weak Mg II absorbers [rest-frame equivalent width $W_r(2796\ \text{Å}) < 0.3$ Å] are not associated with luminous galaxies, although models designed to fit the Lyman series line and the observed lack of Lyman break constrain the metallicity of the absorbing gas to be at least 10% solar. Photoionization models suggest that the structures responsible for weak Mg II absorption might be unstable over astronomical timescales, because of pressure imbalance between a high-density, low-ionization ($p/k = 10^{-5}$ cm^{-3} K^{-1}) and a low-density, high-ionization ($p/k = 10^{-8}$ cm^{-3} K^{-1}) phase (Charlton et al. 2003; Narayanan et al. 2005). The conclusions from photoionization models are based on the observed values of column density and Doppler parameter for the low- and high-ionization transitions. The best constraints on these parameters are mostly from high-resolution data at $R \sim 45{,}000$ or lower. The b-parameters measured at $R \sim 45{,}000$ ($b \sim 2$ or 3 km s^{-1}) allow for temperatures of thousands of kelvins, similar to the temperatures inferred for the high-ionization phases. If the true Doppler parameter is smaller than that derived from the HIRES measurements, then it would imply that the low-ionization phase has a much lower temperature than the high-ionization phase. This influences the inference about their stability. Line widths narrower than ∼2 km s^{-1} ($T < 15{,}000$ K) cannot be accurately measured at $R = 45{,}000$. Therefore, the temperature estimations for the low-ionization phase in these absorbers may not be accurate. Our $R = 120{,}000$ Subaru HDS spectrum allows us to test the assumption that these single-cloud, weak Mg II lines are resolved.

For the two single-cloud, weak Mg II absorbers at $z = 0.9056$ and 0.8181 found in the PG 1634+706 spectrum, we find from the HDS spectrum that the weak Mg II lines are not any narrower than values measured at $R = 45{,}000$ (Fig. 13). The column densities and Doppler parameters from simultaneous Voigt profile fits to Mg II $\lambda\lambda$2796, 2803 are listed in Table 4. Thus, at least for these cases, the lines were already sufficiently resolved at $R = 45{,}000$ to allow measurements of the b-values that were accurate within the errors. These measurements are in concordance

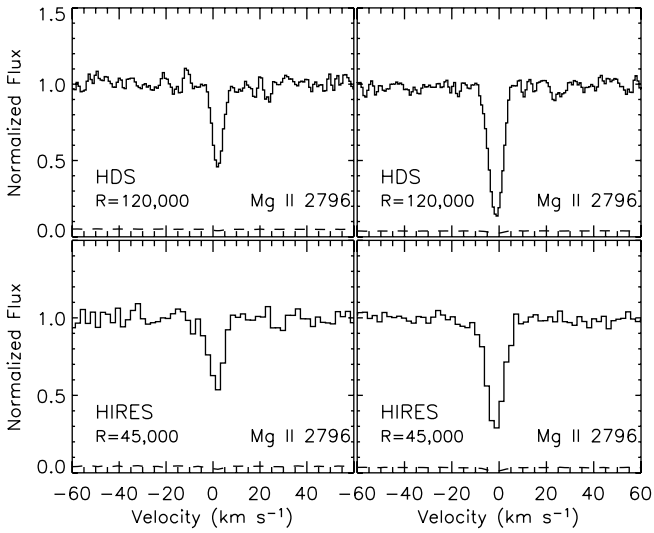

FIG. 13.—Two single-cloud, weak Mg II systems at redshifts 0.8181 (*left panels*) and 0.9056 (*right panels*) as detected in the Keck HIRES and Subaru HDS spectra of PG 1634+706. The dashed lines show the error spectra. The Voigt profile fit results are listed in Table 4.

with the instability inference based on photoionization models. Analogs of weak Mg II absorbers are known to exist in the present-day universe (Narayanan et al. 2005), as well as at intermediate ($z \sim 1$; Churchill et al. 1999) and higher redshifts ($z \sim 2$; Lynch et al. 2006). Therefore, confirming the transient nature of these systems is significant in addressing the question of the evolution of the processes that created these absorbing structures. A larger sample of weak Mg II absorbers should be measured with superhigh resolution in order to verify that we can generalize this conclusion. However, the real value in $R > 100{,}000$ observations in the study of weak Mg II absorbers will be the enhanced sensitivity that will allow us to establish the shape of the distribution function for the weakest absorbers, and to infer their physical properties.

TABLE 4
VOIGT PROFILE FIT RESULTS FOR WEAK Mg II SYSTEMS

Instrument	v (km s^{-1})	log [N(Mg$^+$)] (atoms cm^{-2})	b(Mg$^+$) (km s^{-1})
	$z = 0.8181$ Single-Cloud System		
HIRES.....	0	12.04 ± 0.03	2.14 ± 0.40
HDS.....	0	11.97 ± 0.02	2.61 ± 0.13
	$z = 0.9056$ Single-Cloud System		
HIRES.....	0	12.47 ± 0.01	2.77 ± 0.12
HDS.....	0	12.42 ± 0.01	3.14 ± 0.07
	$z = 1.0414$ Multiple-Cloud System		
HIRES.....	−38.2	11.49 ± 0.08	6.53 ± 1.62
	−15.2	11.90 ± 0.06	10.81 ± 2.03
	0	12.02 ± 0.03	3.12 ± 0.38
	15.7	11.68 ± 0.04	5.95 ± 0.83
HDS.....	−36.4	11.17 ± 0.23	3.98 ± 2.78
	−29.6	10.98 ± 0.27	2.23 ± 1.46
	−17.3	11.38 ± 0.14	5.19 ± 1.99
	−10.1	11.05 ± 0.25	2.35 ± 1.08
	1.9	12.02 ± 0.01	3.82 ± 0.13
	18.0	11.48 ± 0.04	2.86 ± 0.34

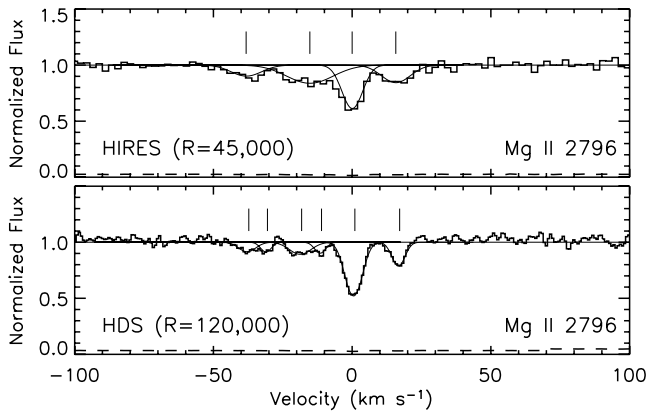

FIG. 14.—Multiple-cloud, weak Mg II system at $z = 1.0414$ as detected in the Keck HIRES and Subaru HDS spectra of PG 1634+706. The thin solid lines superposed on the spectra are the various Voigt profile components contributing to the absorption feature. The vertical lines placed above the features represent the center of each component in the absorption profile. The dashed lines represent the error spectra. The Voigt profile fitting results are listed in Table 4.

3.3. *Multiple-Cloud, Weak* Mg II *Absorbers*

Approximately 35% of weak Mg II absorbers have multiple clouds (Rigby et al. 2002). Based on their kinematics, these multiple-cloud, weak Mg II absorbers can be described as "kinematically compact" or "kinematically spread." The kinematically compact systems have been hypothesized to arise in dwarf galaxies, and the kinematically spread systems in the outskirts of spiral galaxies (Masiero et al. 2005; Ding et al. 2005), but it is likely that the situation is more complicated. Varying degrees of line blending in the absorption features imply that the Voigt profile fit results are sometimes going to be sensitive to resolution. This is illustrated by the $z = 1.0414$, multiple-cloud, weak Mg II system in the spectrum of PG 1634+706. Based on HIRES data, this weak Mg II absorber was classified as a multiple-cloud, weak Mg II system with four discrete Mg II clouds (Churchill et al. 2003). Two additional weak components were resolved in Voigt profile fits to the higher resolution data in the same region, as shown in Figure 14. Zonak et al. (2004) produced models for the system based on the HIRES data along with $R = 30{,}000$ ultraviolet spectra obtained with *HST* STIS. It is apparent from our HDS spectrum in Figure 15 that there are two subsystems in Mg II, separated by ~150 km s^{-1}. For the blueward subsystem (see Zonak et al. 2004), Mg II λ2796 was not covered in the HIRES spectrum and Mg II λ2803 was not detected, but several other metal-line transitions (e.g., Si III λ1207, Si IV $\lambda\lambda$1394, 1403, etc.) were detected in the *HST* STIS spectrum. The greater sensitivity of the $R = 120{,}000$ HDS spectrum led to detection of Mg II λ2803 in the blueward subsystem, which was a prediction of the models of Zonak et al. (2004)

Enhanced resolution allows the detailed shapes of absorption profiles to be surveyed and blends to be separated. Some single-cloud, weak Mg II absorbers appear asymmetric when observed at $R = 45{,}000$ (Churchill et al. 1999), suggesting they may have more than one Voigt profile component. More generally, it is of interest what fraction of the single-cloud, weak Mg II absorbers are truly fitted by single Voigt profile components when viewed at higher resolution. The profiles of the $z = 0.9056$ and 0.8181 systems observed at $R = 120{,}000$ here are still fitted adequately by a single component, suggesting a very simple structure. Observing some asymmetric, single-cloud, weak Mg II may reveal some to be more similar to kinematically compact, multiple-cloud, weak

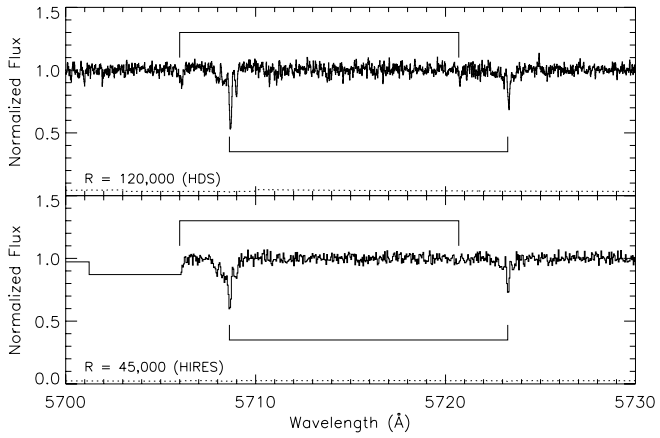

FIG. 15.—The $z = 1.0414$ multiple-cloud, weak Mg II system and the associated subsystem in the spectrum of PG 1634+706. The dotted lines represent the error spectra. The thin solid lines mark the respective positions for the 2796 and 2803 Å lines that form the doublet pair. The two absorption systems are separated by $\sim$150 km s^{-1}. In the HIRES spectrum, for the bluer subsystem the Mg II λ2796 transition was not covered due to an echelle order break. However, the weaker pair of the doublet, Mg II λ2803, was not detected down to an equivalent-width limit of 3 σ. On the other hand, there is a clear detection of this weak subsystem in the HDS spectrum.

Mg II absorbers, or they could just be variations of ordinary, single-cloud, weak Mg II absorbers. Determinations of their metallicities and comparisons of kinematics of other transitions should allow a separation of these classes.

3.4. *Milky Way Absorption and High-Velocity Clouds*

In the HDS spectrum, Galactic Na I is detected, as shown in Figure 16. Voigt profile fitting parameters are listed in Table 5.

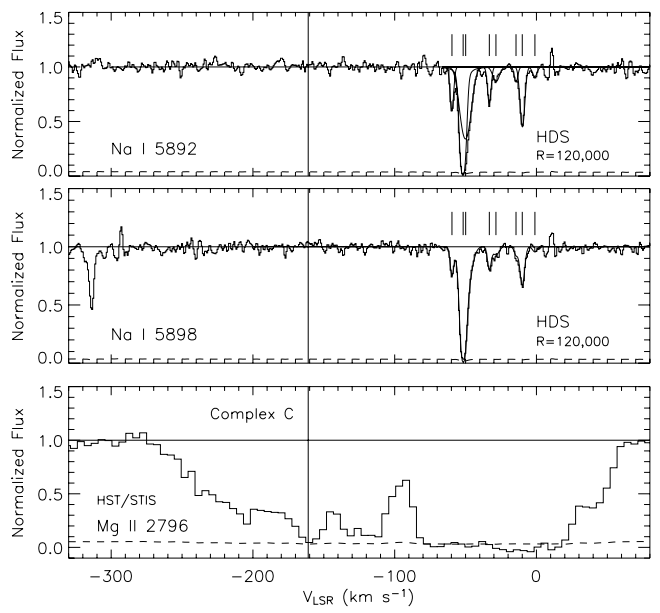

FIG. 16.—Galactic Na I detections in the HDS spectrum of PG 1634+706. The superhigh-resolution spectrum allowed measurements of the b-value of $\sim$1 km s^{-1}. Superposed in thin lines are the various Voigt profile components contributing to the absorption. The vertical lines mark the center of each component. The thin line in the Na I λ5898 panel shows the cumulative Voigt profile by combining the various components. The fit results are listed in Table 5. The Mg II absorption from the HVC complex C along the line of sight to the quasar is also shown. To guide the eye, the expected location of the Na I doublet absorption from the HVC is marked by the vertical line.

TABLE 5

VOIGT PROFILE MEASUREMENT OF GALACTIC Na I ABSORPTION IN THE HDS SPECTRUM OF PG 1634+706

v_{LSR} (km s^{-1})	log [N(Na)] (atoms cm^{-2})	b(Na) (km s^{-1})
−1.1	10.56 ± 0.10	1.68 ± 0.82
−10.0	11.51 ± 0.02	1.63 ± 0.16
−14.4	10.67 ± 0.10	0.89 ± 0.88
−28.6	10.90 ± 0.11	2.80 ± 1.02
−33.2	11.14 ± 0.05	0.90 ± 0.33
−49.9	11.96 ± 0.34	4.64 ± 0.28
−51.7	14.21 ± 1.63	1.02 ± 0.35
−59.6	11.26 ± 0.05	0.86 ± 0.21

For the narrowest component, at $v_{LSR} = -32$ km s^{-1},[4] we measure $b = 0.9 \pm 0.2$ km s^{-1}. This shows that such narrow lines as $b \sim 1$ km s^{-1} can be measured at $R = 120{,}000$. At the same time, we also note that the hyperfine splitting in Na I lines is likely to affect our measurement of such a narrow line width. The difference in rest-frame wavelength from the basic hyperfine splitting of the D1 and D2 lines has been measured to be 0.0213 and 0.0198 Å, respectively (Morton 2003). This corresponds to shifts in velocity of 1.0827 and 1.0075 km s^{-1}, respectively. As these values are very close to our measurement of $b \sim 1$ km s^{-1}, we expect the true b to be lower than this measured value. However, observing this effect by resolving the line would require spectral resolutions that are significantly larger than our HDS measurement at $R = 120{,}000$ (as discussed in § 2.2.)

The PG 1634+706 line of sight passes through the well-studied HVC complex C. On inspection of a *HST* STIS E230M spectrum, we find absorption detected in Mg II, Mg I, and Fe II at $v_{LSR} \sim -115$ and -155 km s^{-1}. We do not detect Na I $\lambda\lambda$5892, 5898 at these velocities in our $R = 120{,}000$ spectrum to a 3 σ limit of 0.004 Å pixel^{-1}. Recently, 21 cm H I observations have found that high-velocity, low column density hydrogen clumps have $T < 900$ K (Hoffman et al. 2004; Richter et al. 2005) and that narrow Ca II lines are detected in most sight lines (Richter et al. 2005). Unfortunately, Ca II $\lambda\lambda$3935, 3970 is not covered in either our $R = 45{,}000$ or $R = 120{,}000$ spectrum of PG 1634+706. However, at $R = 45{,}000$ it would not be possible to test whether the Ca II lines are as narrow as would be suggested by the low temperatures from H I. Thus, the study of HVCs is an application for which superhigh resolution will be particularly valuable. This applies to HVCs around galaxies at high redshift, as well as to Milky Way HVCs.

4. CONCLUSION

The ability to routinely obtain quasar spectra with resolutions of $R > 100{,}000$ is not likely to provide as large a change in the field of quasar absorption lines as the previous advance to $R = 45{,}000$, made possible with 8 m class telescopes. However, the ability to probe structure on scales of $\sim$1 km s^{-1} will certainly be valuable in select applications and in detailed studies of particular absorbers. Examples of such applications include probing the physical conditions of cold regions in the ISM of galaxies, particularly in DLAs and other strong Mg II absorbers. Also, it appears that high-velocity clouds, both around the Milky Way

[4] We adopt the "standard" definition of the local standard of rest (Kerr & Lynden-Bell 1986), in which the Sun is moving in the direction $\alpha = 18^h$, $\delta = +30^\circ$ (epoch 1900) at 20 km s^{-1}. With this convention, the conversion to heliocentric velocity is $v_{helio} = v_{LSR} + 14.770$ km s^{-1}.

and at high redshift, may have a cold phase. Finally, surveys extending to small equivalent widths will be aided by the enhanced sensitivity of higher resolution observations.

Our comparison of $R = 120{,}000$ Subaru HDS observations to $R = 45{,}000$ Keck HIRES observations of various systems toward PG 1634+706 show that at the higher resolution, more accurate Doppler parameter measurements can be made, and that additional Voigt profile components are resolved. However, for the particular Mg II absorbers along the PG 1634+706 sight line no extremely narrow individual components were measured. It was only for the Galactic Na I line in this line of sight that $b < 1$ km s^{-1} was measured. Because such narrow components are expected in a variety of environments, it would be valuable to push the limits of 8 m class telescopes in order to detect these lines in a variety of types of systems toward the brightest quasars.

We are grateful to Chris Churchill for giving us permission to use the Keck HIRES spectrum for this work. We also wish to thank the referee, John Black, for several insightful comments that have increased the scope of this paper.

REFERENCES

Bergeron, J., & Boissé, P. 1991, A&A, 243, 344
Beverini, N., Maccioni, E., Pereira, D., Strumia, F., Vissani, G., & Wang, Y.-Z. 1990, Opt. Commun., 77, 299
Caulet, A. 1989, ApJ, 340, 90
Chand, H., Srianand, R., Petitjean, P., Aracil, B., Quast, R., & Reimers, D. 2006, A&A, 451, 45
Charlton, J. C., & Churchill, C. W. 1998, ApJ, 499, 181
Charlton, J. C., Ding, J., Zonak, S. G., Churchill, C. W., Bond, N. A., & Rigby, J. R. 2003, ApJ, 589, 111
Charlton, J. C., Mellon, R. R., Rigby, J. R., & Churchill, C. W. 2000, ApJ, 545, 635
Churchill, C. W. 1997, Ph.D. thesis, Univ. Santa Cruz
Churchill, C. W., Mellon, R. R., Charlton, J. C., Jannuzi, B. T., Kirhakos, S., Steidel, C. C., & Schneider, D. 2000, ApJ, 543, 577
Churchill, C. W., Rigby, J. R., Charlton, J. C., & Vogt, S. S. 1999, ApJS, 120, 51
Churchill, C. W., & Vogt, S. S. 2001, AJ, 122, 679
Churchill, C. W., Vogt, S. S., & Charlton, J. C. 2003, AJ, 125, 98
Cowie, L. L., Songaila, A., Kim, T. S., & Hu, E. M. 1995, AJ, 109, 1522
Davé, R., Hernquist, L., Katz, N., Weinberg, D., & Churchill, C. W. 1996, BAAS, 188, 23.08
Dekker, H., et al. 2000, Proc. SPIE, 4008, 534
Ding, J., Charlton, J. C., Bond, N. A., Zonak, S. G., & Churchill, C. W. 2003, ApJ, 587, 551
Ding, J., Charlton, J. C., & Churchill, C. W. 2005, ApJ, 621, 615
Elmegreen, B. G. 1997, ApJ, 477, 196
Hoffman, G. L., Salpeter, E. E., & Hirani, A. 2004, AJ, 128, 2932
Kerr, F. J., & Lynden-Bell, D. 1986, MNRAS, 221, 1023
Lane, W. M., Briggs, F. H., & Smette, A. 2000, ApJ, 532, 146
Lanzetta, K. M., & Bowen, D. V. 1992, ApJ, 391, 48
Lanzetta, K. M., Turnshek, D. A., & Wolfe, A. M. 1987, ApJ, 322, 739
Lynch, R. S., Charlton, J. C., & Kim, T. S. 2006, ApJ, 640, 81
Masiero, J. R., Charlton, J. C., Ding, J., Churchill, C. W., & Kacprzak, G. 2005, ApJ, 623, 57
Misawa, T., Tytler, D., Iye, M., Storrie-Lombardi, L. J., Suzuki, N., & Wolfe, A. M. 2002, AJ, 123, 1847
Morton, D. C. 2003, ApJS, 149, 205
Narayanan, A., Charlton, J. C., Masiero, J. R., & Lynch, R. 2005, ApJ, 632, 92
Noguchi, K., et al. 2002, PASJ, 54, 855
Petitjean, P., Srianand, R., & Ledoux, C. 2000, A&A, 364, L26
Points, S. D., Lauroesch, J. T., & Meyer, D. M. 2004, PASP, 116, 801
Richter, P., Westmeier, T., & Brüns, C. 2005, A&A, 442, L49
Rigby, J. R., Charlton, J. C., & Churchill, C. W. 2002, ApJ, 565, 743
Sargent, W. L. W., Boksenberg, A., & Steidel, C. C. 1988, ApJS, 68, 539
Srianand, R., Petitjean, P., Ledoux, C., Ferland, G., & Shaw, G. 2005, MNRAS, 362, 549
Steidel, C. C., Dickinson, M., Meyer, D. M., Adelberger, K. L., & Sembach, K. R. 1997, ApJ, 480, 568
Tappe, A., & Black, J. H 2004, A&A, 423, 943
Vogt, S. S., et al. 1994, Proc. SPIE, 2198, 362
Wolfe, A. M., Prochaska, J. X., & Gawiser, E. 2003, ApJ, 593, 215
Zonak, S. G., Charlton, J. C., Ding, J., & Churchill, C. W. 2004, ApJ, 606, 196